Characterization and catalytic performance of mesoporous molecular sieves Al-MCM-41 materials

Xiaoyin Chen, Limin Huang, Guozhong Ding and Quanzhi Li *

Department of Chemistry, Fudan University, Shanghai 200433, PR China

Received 9 August 1996; accepted 18 December 1996

Mesoporous Al-MCM-41 materials of different Si/Al ratios have been synthesized and characterized by X-ray powder diffraction, ^{27}Al and ^{29}Si MAS NMR, differential thermogravimetric analysis, N_2 adsorption measurements, FT-IR and catalytic cracking of alkanes. The experimental results show that the incorporation of aluminium into the framework of MCM-41 has a great effect on the degree of long-distance order, the surface acidities and the mesoporous structures of the materials. With increase of the aluminium content, the amounts of tetrahedral framework aluminium and the acid sites on the samples increase, but the acid strength decreases. Al-MCM-41 materials exhibit high activity for n-C_{16}^0 cracking and good selectivity for producing low carbon alkylenes, particularly for i-$C_4^=$.

Keywords: Al-MCM-41, characterization, catalytic performance

1. Introduction

The recently developed mesoporous molecular sieves MCM-41 materials have attracted extensive interest because of their large surface areas, uniform pore channels and good thermal stabilities [1,2]. These materials are prospects for applications as adsorbents and catalysts supports. But, for use as acid catalysts, aluminium atoms must be incorporated into the framework of MCM-41. The synthesis and characterization of Al-MCM-41 materials have been reported elsewhere since the first report of synthesis of Al-MCM-41 at Mobil Corporation [2]. Up to now, some aspects of the aluminium source in synthesis, the effect of aluminium incorporation on the structure of framework and pore channel, the distribution and the coordination state of aluminium in Al-MCM-41 materials have been investigated [3–6]. However, only a few papers have focused on the acid properties of Al-MCM-41 and their direct use as catalysts in detail [7–9]. In this paper we describe the characterization of structure, acidity and the catalytic performance of Al-MCM-41 materials with different Si/Al ratios. The relationship between the acidic properties of Al-MCM-41 and the cracking performance of long-chain n-alkanes for producing low carbon alkenes was also discussed.

2. Experimental

2.1. Synthesis of Al-MCM-41

Al-MCM-41 materials with different Si/Al ratios were synthesized according to the general procedure described by Schmidt et al. [10]. The reaction mixtures were composed of sodium silicate, sodium aluminate, cetyltrimethylammonium bromide (CTMAB) and distilled water. The alkalinity of mixtures was adjusted by H_2SO_4 to pH 12. The molar composition of the mixtures was $5SiO_2$:xAl_2O_3:CTMAB:$610H_2O$ with x varying from 0 to 0.5. The formed gel was stirred extensively, then loaded into an autoclave and heated without stirring at 100°C for 144 h. After cooling to room temperature, the resulting solid products with different Si/Al ratios were recovered by filtration, extensively washed with deionized water and dried in air at $\leqslant$80°C. The as-synthesized products were then calcined at 550°C for 1 h in flowing nitrogen and then in air for 6 h.

2.2. The characterization of Al-MCM-41

The powder X-ray diffraction (XRD) patterns were recorded with a Rigaku D/MAX-IIA X-ray powder diffractometer. This diffractometer system employed Ni-filtered Cu Kα radiation and was operated at 40 kV and 20 mA.

The solid-state MAS NMR spectra were recorded at room temperature on a Bruker MSL-300 spectrometer with resonance frequencies of 78.21 MHz for ^{27}Al and 59.63 MHz for ^{29}Si. The magnetic field was 7.05 T. The spin rate of the sample was 4.0 kHz and the number of scans was 1500–2500. The pulse lengths were adjusted to 4.6 and 7.0 μs with repetition times to 500 ms and 1.0 s, respectively. The sweep width was 29411 Hz for ^{27}Al and 20000 Hz for ^{29}Si.

IR spectra were obtained on a Nicolet 5SXC FTIR spectrometer, using self-supporting wafers of 10 mg treated in a vacuum cell at 400°C and 3×10^{-3} Pa for 4 h.

* To whom correspondence should be addressed.

The IR spectra of the samples before pyridine adsorption were recorded after the temperature decreased to 300°C. Pyridine was then admitted at room temperature, and after equilibrium the samples were degassed at higher temperatures of 100°C, 200°C and 300°C, respectively, to remove adsorbed pyridine. Then the spectra of pyridine for in situ thermal desorption were recorded.

Surface areas and N_2 adsorption–desorption isotherms on the samples were measured on an ASAP-2000 apparatus using nitrogen as adsorbate at −196°C. The pore structural data were analyzed by the BJH method with the Halsey equation for multilayer thickness.

Differential thermogravimetric (DTG) analysis was performed on a Rigaku PTC-10A. After flowing argon gas of 40 cm^3/min for 2 h, the samples were heated with a heating rate of 10°C/min from room temperature to 850°C. The bulk chemical composition was determined by chemical analysis using the volume method of potassium fluoride and EDTA titration.

The catalytic cracking reactions of n-C_{16}^0, n-C_{12}^0, n-C_{10}^0, n-C_7^0 were performed in a pulse microreactor at temperature of 510°C with N_2 flow rate of 15 ml/min. Catalysts of 100 mg were put into a quartz tube with diameter of 4 mm. For n-C_{16}^0 cracking on Al-MCM-41 with different aluminium contents, similar conversions were obtained by varying the amount of the catalysts applied. The reaction products were analyzed on a gas chromatograph with OV-101 glass capillary column of 50 m and gas products were analyzed by a squalane/γ-Al_2O_3 column of 3 m. FID was used as detector.

3. Results and discussion

3.1. The distribution and coordinate state of aluminium in MCM-41

Fig. 1 shows XRD patterns of calcined MCM-41 materials with different Si/Al ratios. The d_{001} spacings are shown in table 1. It can be noted that purely siliceous MCM-41 exhibits the typical hexagonal lattice corresponding to that reported by Beck et al. [2]. It shows three low-angle peaks in the region $2\theta = 1°-8°$, corresponding to reflections at 3.67, 2.16 and 1.87 nm. However, for the aluminium-containing MCM-41 only the (100) diffraction peak is obtained and the weak diffractions corresponding to the (110) and (200) peaks at higher angle are difficult to resolve. Pinnavaia et al. and others have demonstrated that similar single diffractions of MCM-41 type materials still exhibit crystallographic symmetry analogous to MCM-41 phases [11]. With the decrease of the Si/Al ratio or the increase in aluminium content of the samples, the spacing of the (100) peak increases from 3.67 nm of purely siliceous MCM-41 to 4.41 nm of aluminium MCM-41 with Si/Al ratio of 10. The observed increase in the interplanar spacing can be explained by the increase in wall thickness ($t = a - d_p$, $d_{100} = a \sin 60°$) of MCM-41 materials (see table 1) and/or on the basis of replacement of shorter Si–O bonds (0.160 nm) by longer Al–O bonds (0.175 nm) in the MCM-41 structure [5]. On the other hand, with the increase in aluminium content of the samples the (100) diffraction peak becomes broader and less intense. It is suggested that the change of the T–O–T bond angle due to aluminium incorporation into the framework structure of MCM-41 results in a distortion of the long-range ordering of the hexagonal mesoporous structure and the disappearance of the (110) and (200) diffractions.

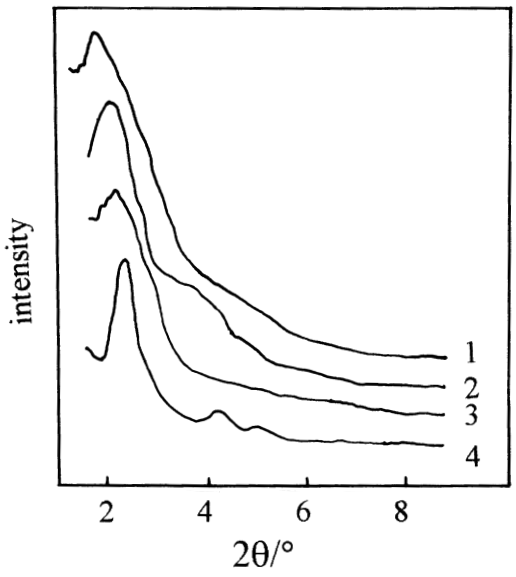

Fig. 1. Power X-ray diffraction patterns of calcined Al-MCM-41: samples 1, 2, 3 and 4.

The ^{29}Si MAS NMR spectra of Al-MCM-41 are shown in fig. 2. These spectra also indicate the incorporation of aluminium into the MCM-41 framework. For the purely siliceous MCM-41, we can clearly observe the well resolved main peaks of the Q^4 (−110.3 ppm, Si(4OSi)) and Q^3 (−100.9 ppm, Si(3OSi)OH) units and the weak peak of the Q^2 (−90.6 ppm, Si(2OSi)$(OH)_2$) unit, corresponding to area percentages of 58, 36 and 6, respectively. The resolution of ^{29}Si spectra of sample 1 decreases due to the incorporation of Al into MCM-41 structure. But three ^{29}Si peaks (−107.0, −100.5, −90.0 ppm) can also be obtained by Gaussian simulation, corresponding to percentages of 36, 48 and 16,

Table 1
Comparison of samples with different Si/Al ratios

Sample	Si/Al (gel)	Aluminium content [a] (wt%)	d_{100} (nm) calcined
1	10	4.84	4.41
2	50	0.83	4.33
3	100	[b]	4.01
4	∞	[b]	3.67

[a] From chemical analysis.
[b] Beyond the analysis limits.

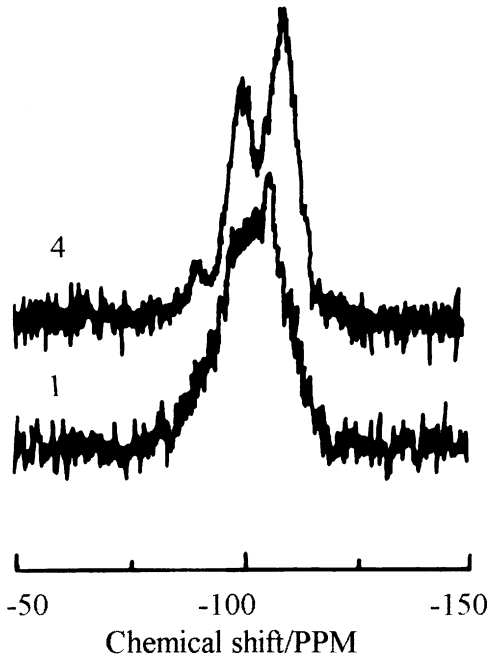

Fig. 2. ^{29}Si MAS NMR of calcined sample 1 and sample 4.

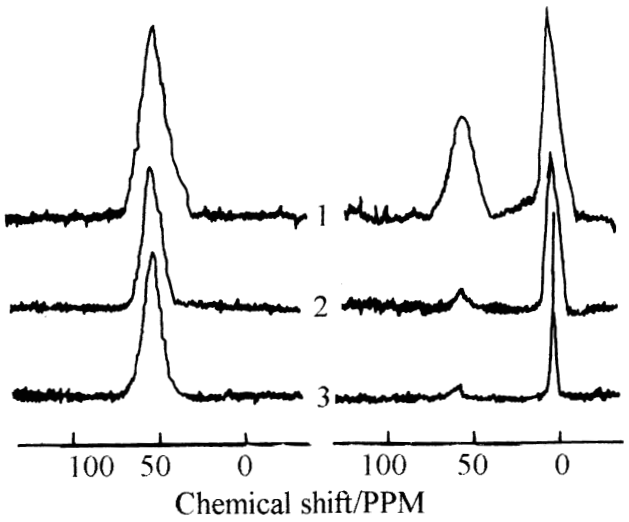

Fig. 3. ^{27}Al MAS NMR of uncalcined (left) and calcined (right) Al-MCM-41: samples 1, 2 and 3.

respectively. In comparison with those of purely siliceous MCM-41, the peak intensity of Q^4 for Al-MCM-41 decreases, but the peak intensities of Q^3 and Q^2 increase. On the basis of results obtained by Gaussian simulation, the increase of percentage of Q^3 probably results from the overlapping of the Q^3 (0Al) peak and the Q^4 (1Al) peak, and Q^2 from the overlapping of the Q^2 (0Al) peak and the Q^3 (1Al) peak. The results of ^{29}Si NMR spectra not only demonstrate the incorporations of aluminium atoms into the mesoporous framework structure, but also reveal the distributions of aluminium atoms in the MCM-41 framework structure. The spectra of solid state ^{27}Al MAS NMR further indicate that the aluminium atoms are coordinated into the Al-MCM-41 framework, as shown in fig. 3. In ^{27}Al spectra, the peaks around 50 and 0 ppm can be assigned to the chemical shift of tetrahedrally coordinated aluminium in framework and octahedral non-framework aluminium, respectively [4–6]. We note that all uncalcined samples exhibit only a peak at 53.0 ppm corresponding to tetrahedrally coordinated framework aluminium. With the increase of the aluminium content, the peak becomes broader, which probably results from secondary quadrupole interaction of the aluminium species or the presence of aluminium in an environment with a low symmetry. After calcination at 550°C, we can observe that the intensities of peaks of tetrahedrally coordinated aluminium decrease and the peaks corresponding to octahedral non-framework Al species appear for all samples. It indicates that the dealumination occurs for all Al-MCM-41 with the removal of template and the thermal stability of tetrahedrally coordinated framework aluminium is poor. However, we can still observe the peaks of tetrahedrally coordinated aluminium for all calcined samples and the intensities of these peaks increase with increasing aluminium content.

3.2. Surface area and mesopore distribution of Al-MCM-41

Fig. 4 shows the N_2 adsorption–desorption isotherms of the samples. In accord with those of MCM-41 materials, all samples exhibit a well-expressed hysteresis loop

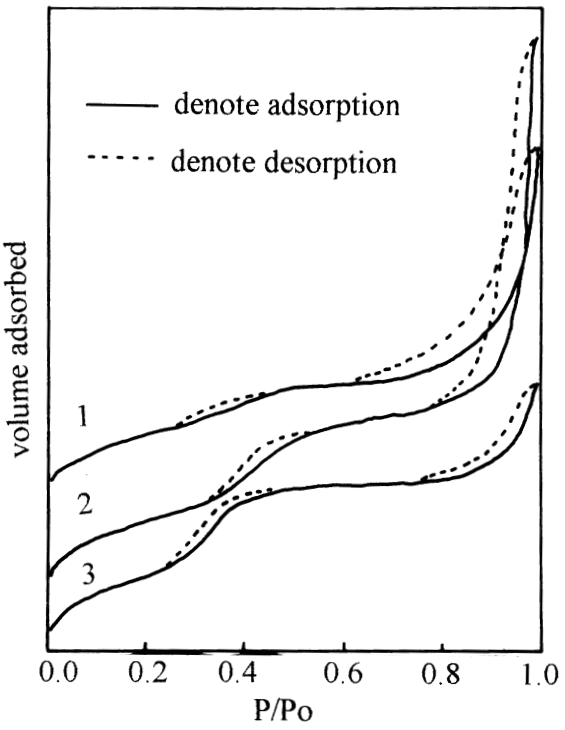

Fig. 4. Adsorption isotherms of nitrogen on samples 1–3 at −196°C.

at $P/P_0 \approx 0.4$, which is indicative of framework-confined mesopores. Table 2 shows pore structural data of the Al-MCM-41 samples, which were obtained by nitrogen physisorption. We note that the specific surface area and pore volume in the mesopore region of 1.7 to 4.0 nm decrease with the increase of the aluminium content. The decrease in the mesopore surface area and volume can be explained by the increase of the wall thickness of Al-MCM-41 materials and/or by the dealumination of framework during calcination. The higher the content of aluminium in the sample is, the less the mesopore surface area and pore volume is. From table 2 it can also be seen that the ratios of mesopore surface areas to total surface areas are 66.1, 69.2 and 92.6%, respectively, for samples 1, 2 and 3, indicating that the mesopore structures for all Al-MCM-41 samples are still dominant. The percentage of mesopore surface area in total surface area increases with the increase of Si/Al ratio, suggesting that the size of mesopores for the sample with low aluminium content is more uniform than that for the sample with high aluminium content. From these results we can conclude that adding aluminium in the synthesis system will result in scattering of the mesopore distribution. With the increase of the aluminium content the effect of the scattering becomes more apparent resulting in poorly hexagonal crystalline materials, which is in agreement with the results of XRD. By comparison of the values of S_m and V_m in the mesoporous range (1.7–4.0 nm). with S and V of the total pore range (1.7–100 nm), it can be seen that the ratio of V_m/V is lower than that of S_m/S for all samples due to the effect of pores formed between crystallites. These larger pores formed between crystallites contribute more pore volume than pore surface area.

3.3. Acidic properties of Al-MCM-41

The IR spectra, obtained from in situ results of all samples in the vibrational range of hydroxyl groups, show a very intense band at 3740 cm^{-1} which corresponds to terminal silanol groups, and a wide band at 3628 cm^{-1} which can be assigned to a hydroxyl groups vibrational band related to Al species (see fig. 5). The vibrational intensity of the hydroxyl group at 3628 cm^{-1} increases with the increase of aluminium content. From the results corrected by subtracting the spectra before pyridine adsorption from those after pyridine adsorption, it can be concluded that both hydroxyl groups are responsible for the surface acid sites of the samples. By comparing the intensities of the hydroxyl groups after adsorption of pyridine with those before adsorption of pyridine for all samples, we can note that the intensities of the former peaks are much lower than those of the latter. It suggests that the acidic hydroxyl groups predominate for Al-MCM-41 materials. With the increase of the desorption temperature of pyridine the intensities of both peaks decrease fast, indicating that the strengths of acid sites for Al-MCM-41 are weak. Fig. 6 shows IR spectra of the pyridine adsorbed on samples with differ-

Table 2
Nitrogen physisorption data of MCM-41 samples

Sample	Surface area (m^2/g)			Pore volume (cm^3/g)		
	S_m [a]	S [b]	S_m/S (%)	V_m	V	V_m/V (%)
1	511.9	774.8	66.1	0.328	1.261	26.0
2	686.7	992.5	69.2	0.499	1.942	25.7
3	1093.5	1181.4	92.6	0.714	1.085	65.8

[a] From BJH cumulative desorption of pores at 1.7 to 4.0 nm.
[b] From BJH cumulative desorption of pores at 1.7 to 100.0 nm.

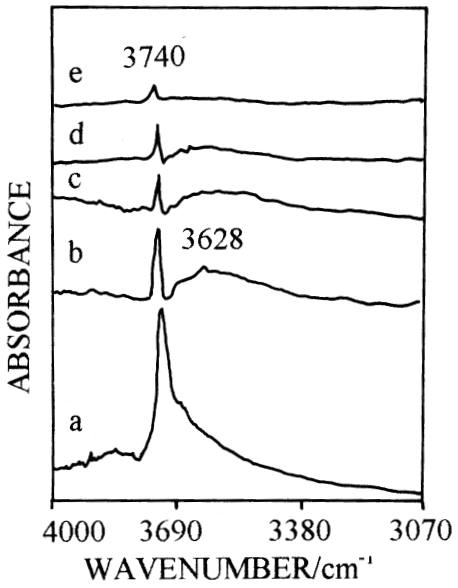

Fig. 5. IR spectra of hydroxyl range before pyridine adsorption on sample 1 (a) and after pyridine adsorption on samples 1, 2, 3 and 4 at 100°C.

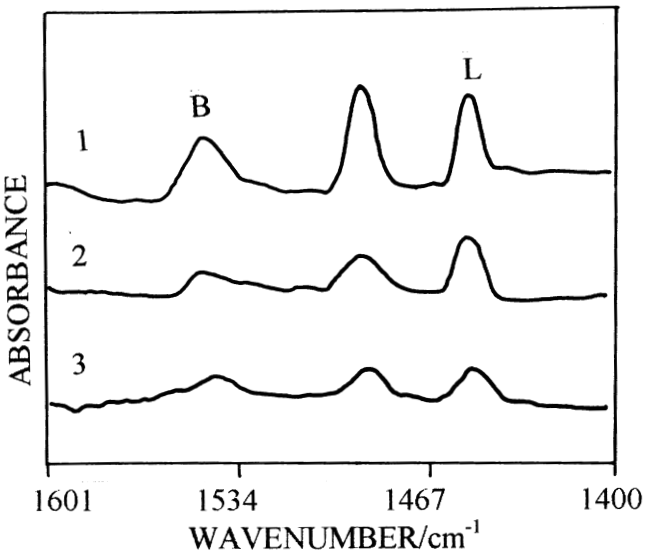

Fig. 6. IR spectra of pyridine adsorbed on samples 1–3 and degassed at 200°C.

Table 3
Acidic amounts of Al-MCM-41 samples. (Py adsorption number at 200°C, 300°C, respectively)

Sample	n_B ($\times 10^{19}$/g) [a]		n_L ($\times 10^{19}$/g) [a]		n_{B+L} ($\times 10^{19}$/g)	
	200°C	300°C	200°C	300°C	200°C	300°C
1	1.57	0.21	2.28	0.43	3.85	0.64
2	1.25	0.33	2.54	0.87	3.79	1.20
3	0.84	0.47	1.51	0.99	2.35	1.46

[a] From extinction coefficient by Hughes and White [12].

ent Si/Al ratios. From the IR spectra of pyridine adsorption, it can be seen that all samples exhibit both Brønsted (band at 1540 cm^{-1}) and Lewis acid sites (band at 1450 cm^{-1}). The quantitative results for both acid sites are listed in table 3. With the increase of the aluminium content of the samples, the amount of Brønsted and Lewis acid sites both increase, while their acid strengths decrease, if comparing the amount of pyridine adsorption at 200 and 300°C, respectively. In combination with ^{27}Al MAS NMR results of the samples (fig. 3) is it indicated that Brønsted acid sites in Al-MCM-41 correspond to framework aluminium, and framework or non-framework aluminium probably contributes Lewis acid sites.

The experimental results of differential thermogravimetric analysis of Al-MCM-41 samples are shown in fig. 7. The weight losses of materials include two parts: the desorption of water and the desorption or decomposition of templates. Peak III and peak IV in fig. 7 can be assigned to desorption of organic templates associated with Si–O^- groups and Brønsted acid sites, respectively [2]. The Si–O^- groups are stronger bases (because Si–OH groups are weaker acids) and should promote Hoffmann elimination at lower temperature ($T_{mIII} \approx 240$°C) corresponding to peak III giving $C_{16}H_{32}$ and $(CH_3)_3N$. The removal of surfactants associated

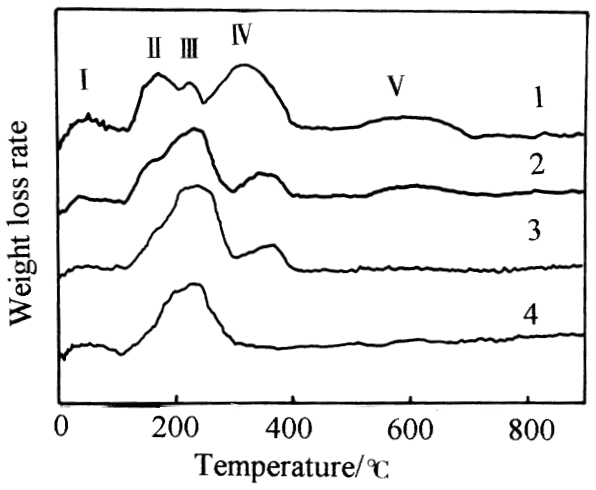

Fig. 7. DTG curves of as-synthesized Al-MCM-41: samples 1, 2, 3 and 4.

Table 4
Thermogravimetric analysis of Al-MCM-41 samples

Sample	Peak III		Peak IV		S_{III}/S_{IV}
	T_m(°C)	weight loss (%)	T_m(°C)	weight loss (%)	
1	259	5.6	363	18.5	0.303
2	248	22.9	367	10.5	2.180
3	237	26.1	381	10.1	2.584

with Brønsted acid sites corresponding to peak IV needs higher temperature ($T_{mIV} \approx 370$°C). With the increase of aluminium content, the percentage of weight loss of peak III decreases but that of peak IV increases, indicating the increase in the amount of Brønsted acid sites (table 4). However, the T_{mIV} shifts from 381 to 360°C, indicating that the Brønsted acid strength decreases with the increase of the Al content.

Generally, cracking of *n*-alkanes with shorter alkyl chains needs catalysts with stronger acid sites. In this paper we have studied the cracking of *n*-alkanes with different long alkyl chains as probe reactions in order to investigate the acid strengths of Al-MCM-41 materials. From experimental results (table 5) we can find that all samples exhibit good activities for *n*-C_{16}^0 cracking, but for *n*-alkanes with the number of carbon of alkyl chains $\leqslant 12$ the cracking activities decrease greatly. The order or cracking activity for these alkanes is described as follows: $C_{16}^0 \gg C_{12}^0 > C_{10}^0 > C_7^0$, indicating that the acid strengths are weak for all Al-MCM-41 materials synthesized. Compared with the cracking activities for sample 3, sample 1 exhibits poorer reactivity for *n*-C_7^0 and *n*-C_{10}^0 but better activity for *n*-C_{16}^0 due to its greater number of acid sites. This can also be seen more clearly by using the ratio of C_{16}^0 conversion to C_{10}^0's or C_{16}^0 conversion to C_{12}^0's as an indicator for acid strength to some extent. The value array is: sample 1 $\ll$ sample 2 $<$ sample 3, which is also the order for acid strength of these samples. For sample 2, because its acid number and strength are medium it shows the highest cracking activities for all *n*-alkanes among Al-MCM-14 materials. From the above results it can be concluded that, with increasing aluminium content, the amount of surface acid sites increases and the acid strength decreases for Al-MCM-41 materials, which is in excellent agreement with the results reported for Py-IR and DTG.

Table 5
The cracking activity of Al-MCM-41 mesoporous materials

Sample	Conversion (%)				$C^a(C_{16}^0)/C(C_{12}^0)$	$C^b(C_{16}^0)/C(C_{10}^0)$
	C_{16}^0	C_{12}^0	C_{10}^0	C_7^0		
1	45.6	5.4	1.0	0.9	8.4	45.6
2	56.2	8.4	7.0	2.4	6.7	8.0
3	36.8	7.3	6.8	2.4	5.0	5.4

[a] Representing the ratio of C_{16}^0 conversion to C_{12}^0's.
[b] Representing the ratio of C_{16}^0 conversion to C_{10}^0's.

Table 6
Cracking performances of n-C_{16}^0 over Al-MCM-41 samples

Sample	Conversion (%)	Selectivity (%)			Selectivity of gas products			
		gas ($\leqslant C_4$)	$C_2^=$–$C_4^=$	i-$C_4^=$	olefin (%)	$C_2^=$: $C_3^=$: $C_4^=$	$C_4^0/C_4^=$	i-$C_4^=/TC_4^=$
1	45.6	50.9	45.9	14.6	90.1	3 : 39 : 58	0.14	0.55
2	42.6	54.6	48.5	15.7	88.8	4 : 42 : 54	0.12	0.60
3	38.5	55.7	51.2	16.8	91.9	4 : 42 : 54	0.089	0.61

3.4. Catalytic activities of Al-MCM-41 materials for producing low carbon alkenes

We have also investigated the catalytic performances of Al-MCM-41 materials for producing low carbon alkenes at similar conversions of n-C_{16}^0 ($42 \pm 3\%$). The experimental results are listed in table 6. Because of their low value of the $C_4^0/C_4^=$ ratio responding to the activity of hydrogen transfer reaction, the selectivities of alkenes in total gas phase products are ca. 90% and the selectivities of total gas phase alkenes are between 45% and 51% in all products for all samples. Among the ratios of alkenes in gas phase products, the $C_3^=$ and the $C_4^=$ are the main products and the percentage of $C_4^=$ is the highest, being more than 50%. But that of $C_2^=$ is the lowest, being less than 4%. Thus the selectivity of i-$C_4^=$ can reach up to 16.8% in all cracking products. For sample 2 and sample 3 with higher acid strength but lower acid number, the contents of alkenes in gas phase products are higher than that of sample 1 with weaker acidity. In summary, although the acidities of Al-MCM-41 materials are weak, they are sufficient to cracking alkanes with long alkyl chains, and because of their large surface areas, low density of acid sites and low activities of hydrogen transfer reactions, Al-MCM-41 materials will probably become good potential catalysts for producing low carbon alkenes, particularly for i-$C_4^=$.

It is worth pointing out that, although Al-MCM-41 synthesized using $NaAlO_2$ contains more octahedral Al, it has higher cracking activity than that synthesized using $Al_2(SO_4)_3$ with similar Si/Al ratio, in which only tetrahedral Al is present. This may be due to the reactivity of different Al resources and the interaction between framework Al and non-framework Al to a certain extent. These results will be discussed in later paper.

4. Conclusions

We have synthesized mesoporous molecular sieves Al-MCM-41 materials with different Si/Al ratios. All aluminium atoms in the as-synthesized samples are in the locations of tetrahedral coordinations. After calcination at 550°C, the tetrahedrally coordinated aluminium partially transfers to octahedral aluminium with the removal of organic template, and the degree of order of material with hexagonal array decreases compared with that of purely siliceous MCM-41. With the increase in the content of aluminium, the amount of acid sites increases, while their surface acid strengths decrease, as well as the mesoporous specific surface areas and the mesoporous volumes. Because of large surface areas, low density of acid sites and low activities of hydrogen transfer reactions, Al-MCM-41 materials will probably become good potential catalysts for producing low carbon alkenes, particularly for i-$C_4^=$.

Acknowledgement

Financial supports from the National Nature Science Foundation of China and Postdoctoral Science Foundation of China are gratefully acknowledged.

References

[1] C.T. Kresge, M.E. Leonowicz, W.J. Roth, J.C. Vartuli and J.S. Beck, Nature 359 (1992) 710.
[2] J.S. Beck, J.C. Vartuli, W.J. Roth, M.E. Leonowicz, C.T. Kresge, K.D. Schmitt, C.T.W. Chu, D.H. Olson, E.W. Sheppared, S.B. McCullen, J.B. Higgins and J.L. Schlenker, J. Am. Chem. Soc. 114 (1992) 10834.
[3] M. Janicke, D. Kumar, G.D. Stucky and B.F. Chmelka, Stud. Surf. Sci. Catal. 84 (1994) 243.
[4] R. Schmidt, D. Akporiaye, M. Stocker and O.H. Ellestad, Stud. Surf. Sci. Catal. 84 (1994) 61.
[5] R.B. Borade and A. Clearfield, Catal. Lett. 31 (1995) 267.
[6] K.R. Kloetstra, H.W. Zandbergen and H. van Bekkum, Catal. Lett. 33 (1995) 157.
[7] A. Corma, A. Martinez, V. Martinez-Soria and J.B. Monton, J. Catal. 153 (1995) 25.
[8] R. Mokaya, W. Jones, Z. Luan, M.D. Alba and J. Klinowski, Catal. Lett. 37 (1996) 113.
[9] A. Corma, M.S. Grande, V. Gonzalez-Alfaro and A.V. Orchilles, J. Catal. 159 (1996) 375.
[10] R. Schmidt, D. Akporiaye, M. Stocker and O.H. Ellestad, J. Chem. Soc. Chem. Commun. (1994) 1493.
[11] P.T. Tanev, M. Chibwe and T.J. Pinnavaia, Nature 368 (1994) 321.
[12] T.R. Hughes and H.M. White, J. Phys. Chem. 71 (1967) 2192.